Proceedings of Shanghai 2017
Global Power and Propulsion Forum
30th October – 1st November, 2017
http://www.gpps.global

GPPS-2017-0049

ON THE OFF-DESIGN PERFORMANCE OF SUPERCRITIAL CARBON DIOXIDE POWER CYCLES

Ingo H J Jahn
Centre for Hypersonics
University of Queensland
i.jahn@uq.edu.au
St Lucia, Queensland, Australia

Joshua A Keep
Queensland Geothermal Energy Centre of Excellence
University of Queensland
j.keep @uq.edu.au
St Lucia, Queensland, Australia

ABSTRACT

Cycle modelling is a critical task for the selection of the optimal power cycle configuration for a given nominal operating point and application. With the current trend of increased penetration of renewables in the electricity market, there is increasing importance for a cycle to operate with a high turn down whilst maintaining acceptable thermal efficiency. Thus there is increased need for accurate models for the on and off-design analysis of cycles. Through evaluating cycle performance for changing output requirements and changing ambient conditions it is possible to identify configurations to optimise overall power generation.

This paper presents the results of an investigation into the off-design and part-load operation of the supercritical carbon dioxide (sCO_2) recuperated Brayton and recompression Brayton cycle. The cycle model takes full account of the operating and performance characteristics of the turbomachinery and heat exchanger components and how their performance is affected by changes in cycle operating conditions. This is achieved by modelling the components using physics based approaches or using experimentally determined performance maps scaled to the current applications.

The analysis shows that adjusting the compressor speed is an effective way to modulate the cycle output power. Without additional modifications of the compressors power can be reduced down to 55%, while at the same time cycle efficiency reduces by less than 2 percentage points. This demonstrates the suitability of the sCO_2 cycles for applications that require substantial operation away from the design point, for example in applications that require load following or extended part load operation. In contrast reducing turbine inlet temperature is very detrimental to cycle operation, leading to reduction in thermal efficiency of approximately 1 percentage point per 20K.

Analysis of the off-design operating points of the turbomachinery components also reveals new insight towards setting their nominal conditions and the desired shape of performance maps.

INTRODUCTION

Thermal power conversion cycles, using supercritical carbon dioxide (sCO_2) were first proposed by Angelino (1968). CO_2 has a critical point just above typical ambient temperatures (31.10C), allowing the design of supercritical Brayton cycles. Benefiting from the non-linear thermophyscial properties of sCO_2, these cycle achieve thermodynamic efficiencies better than comparable steam Rankine cycles at temperatures above 500-6000C as shown by Dostal (2014). Turchi et al (2013) showed that with appropriate enhancements, such as introduction of re-compression, cycle efficiencies in excess of 50% can be attained. Further benefits of the supercritical fluid are high densities and low viscosities, which results in compact and power dense components.

As part of the international effort to limit global warming a concerted effort is underway to increase the use of clean and renewable energy sources (United Nations 2016). As a significant portion of the renewable energy sources are intermittent (e.g. Photo Voltaic (PV) and wind) this has created a demand for power systems that are despatchable and that can operate across a wide range of output power (Denholm 2011). Effectively, a system that can follow the demand and quickly compensate for increases in demand or decreases in energy provided from other renewables. Using concentrated solar thermal + thermal storage + sCO_2 power cycle is one of the solutions that addresses the despatchability at a competitive cost (Aghaeimeybodi 2016). In Australia the Australian Solar Research Institute (ASTRI) is investigating such systems in the 1-25MW range as a solution to provide electricity to rural communities (ASTRI 2012). A number of other sCO_2 power system demonstration

projects are currently under way in the USA (Held 2014, Moore et al 2015, Wilkes et al 2016). For applications in this power range, specific speeds in the range 0.2 to 0.6 are typical and radial turbomachinery is a preferred solution (Balje 1962).

A key step during the design of any power system is cycle modelling, which provides the ability to predict performance and allows appropriate cycle operating conditions (pressures, temperature, mass flow rates) to be determined. These results then provide the starting point for detailed component design. Cycle modelling is also applied to investigate operation at off-design conditions. The operation of sCO_2 power cycles with varying boundary conditions, particularly compressor inlet temperature has been investigated previously by a number of authors (Duniman 2017, Sauret 2017, Luu 2017).

Currently a number of cycle modelling tools exist; either those taken from the process industry, i.e. ASPEN, IPSEPro, or those developed specifically for power systems (NPSS, 2017). A further tool is the Steady State Cycle AnalyseR (SSCAR) developed at the University of Queensland (Jahn 2017c). A key capability of SSCAR is the incorporation of turbomachinery performance maps. This allows the tool to predict how the respective operating points are affected by changes in cycle boundary conditions.

The aim of this paper is to presents results from an analytical investigation using SSCAR to provide new insight towards the off-design performance of sCO_2 Brayton cycles and to show that they are able to operate at high turn down ratios (reduction in output power), while maintaining high thermal conversion efficiencies. At the same time the work highlights how the operating point of the turbomachinery components is affected by off-design operation, which is useful insight in regards to setting the nominal design point in order to maximise performance retention and to maximise the operating range.

In the next section the approach employed to model the sCO_2 cycles and the cycle components is described. This is followed by a brief investigation assessing the off-design performance of a recuperated sCO_2 Brayton cycle to illustrate the operation. As the main part of the paper two sCO_2 recompression cycle configurations with different assumed cycle efficiencies are investigated to illustrate their off-design operation and performance.

METHODOLOGY

In order to more completely investigate the off-design performance of power cycles, the Steady State Cycle AnalyseR (SSCAR) was created (Jahn 2017c, Jahn and Keep 2017). SSCAR consists of a main solver and a library of standard thermodynamic components that are linked to form cycle configurations that are analysed for varying boundary conditions (e.g. temperature of heat source and heat sink) and different cycle operating conditions (e.g. shaft speed). Currently the following components are modelled: Turbine, Compressor, Heat Source/Sink, Recuperator, Merge, and Pipe.

To allow on and off-design performance evaluation, of a given cycle configuration all the components are modelled using physics based relationships or performance maps. The software uses the fluid property database CoolProp to obtain appropriate sCO_2 thermophysical properties (Bell et al 2014). The following sections describe the individual component models.

Compressor

A particular advantage of the sCO_2 cycle is that the working fluid can be compressed near the critical point in the supercritical fluid region. Here the non-linear thermophyscial properties allow efficient compression. These effects must be considered when designing and modelling the performance of compressors. To facilitate efficient cycle evaluation the sCO_2 compressor are modelled using a pre-defined performance centrifugal compressor maps, as shown in Fig. 1, which relates shaft speed, enthalpy rise, and isentropic efficiency at a reference condition.

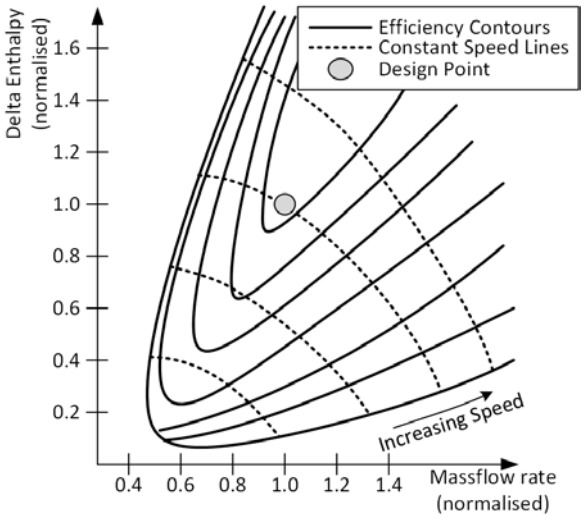

Figure 1: Operating Map for Compressor at reference condition, showing corrected mass flow rate and enthalpy increase.

To account for operation at inlet conditions away from the reference condition, mass flow rate, speed, and enthalpy rise are converted to corrected conditions using the relationships from Glassman (1972).

$$\dot{m}_{corr} = \dot{m}\sqrt{\left(\frac{1}{P}\,V_{cr}\right)}\,\frac{P_{corr}}{P_{in}}\,\epsilon, \qquad (1)$$

$$N_{corr} = N\,V_{cr}, \qquad (2)$$

$$h_{corr} = h\,V_{cr}, \qquad (3)$$

where V_{cr} and ϵ are a specific heat ratio parameter and scaling parameter respectively, as defined in Glassman(1972). As V_{cr} and ϵ incorporate specific heat ratios γ_{in} and γ_{corr} this approach also accounts for fluids with non-ideal properties.

When solving the compressor performance, the mass flow rate and rotational speed are first used to find corresponding enthalpy rise from a performance map. Next

using mass flow rate and enthalpy rise the corresponding efficiency is obtained from the second map. With enthalpy rise and efficiency values, the compressor exit conditions are evaluated using isentropic relations.

Published performance data exists for centrifugal compressors designed by Wright et al (2010) and Clementoni (2015). For the current paper these maps have been scaled in regards to mass flow rate, enthalpy rise, and efficiency to achieve the desired compressor design points. As primary factors (stage Mach number and pressure ratio or specific speed) can be maintained through appropriate geometry selections, the scaled maps are representative. Some changes in performance (map shape) are expected due to change in Reynolds number, but these are generally secondary (Whitfield 1990). Thus using these experimentally determined maps for centrifugal sCO_2 compressors will be representative of larger compressors designed in the future.

Turbine

For the power range (*1-25MW*) considered in this paper, radial inflow turbines are a plausible solution. The performance of these turbines can be characterised by two relationships relating mass flow rate and expansion ratio and efficiency and spouting velocity as shown in Fig. 2 (Whitfield 1990, Glassman 1972).

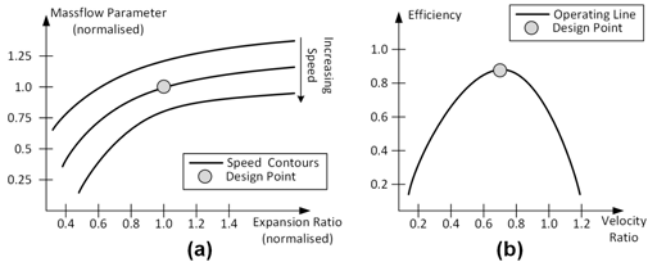

Figure 2: Maps of mass flow parameter (a) and efficiency (b) for radial inflow turbine.

Thus the performance of a radial inflow turbine can be estimated by first calculating the mass flow parameter and equivalent speed

$$MFP = \dot{m}\,\frac{\sqrt{T_{in}}}{P_{in}}, \qquad (4)$$

$$N_{eq} = N\,\sqrt{\frac{T_{in}}{T_{design}}}. \qquad (5)$$

Then by using an appropriate map as shown in Fig. 2(a) the corresponding expansion ratio can be established. Next the isentropic relationships can be used to determine the spouting velocity and velocity ratio

$$C = \sqrt{2\,C_P\;T_{in,total}\left(1-\left(\frac{P_{out}}{P_{in,total}}\right)^{\frac{\gamma-1}{\gamma}}\right)}, \qquad (6)$$

$$\frac{U}{C} = \frac{U}{C}\Big|_{design}\;\frac{N}{N_{design}}\;\frac{C}{C_{design}}. \qquad (7)$$

Using the velocity ratio, the isentropic efficiency can be obtained using the relationship in Fig. 2(b) and actual turbine performance parameters can be calculated using the corresponding isentropic relationships. As sCO_2 turbines typically operate away from the critical point, these ideal gas based relations can be used without introducing significant errors.

For the current study, the turbine performance maps are based on data from a study by Hiett and Johnston (1963), who published geometries and performance maps for a range of radial inflow gas turbines developed and tested by Ricardo & Co. The A70 turbine design has been selected for the present study due to its geometric similarity to power generation turbines, and similarity in pressure ratio and stage Mach number to the turbines employed for sCO_2 demonstrations. Similar to the compressor, the design point of this turbine has been scaled to match the desired cycle operating conditions. This will introduce some absolute errors, however the trends in how a radial turbine responds to changes in speed, mass flow rate, and inlet conditions will be conserved.

Heat Source, Heat Sink, Recuperator

A common method of modelling the performance of heat exchange systems is to use the overall heat transfer coefficient, U, which allows the heat transfer to be calculated as

$$Q = U\,A_R\,\Delta T, \qquad (8)$$

where A_R is an effective area and ΔT is a representative effective area and a corresponding temperature difference. By using multiple axial slices (see Fig. 3) this approach approach can be accurately used for fluids with changing thermal properties and to assess the total $U\,A$ required to achieve a given heat exchanger effectiveness. However, this approach is opaque in regards to identifying the underlying physical effects that drive heat transfer. As such it is not suitable to identify the change in performance of a given heat exchanger arrangement (geometry and size) as boundary conditions for the heat exchanger (temperature, pressure, flow rates) are altered. Being able to capture these effects is essential for off-design performance modelling.

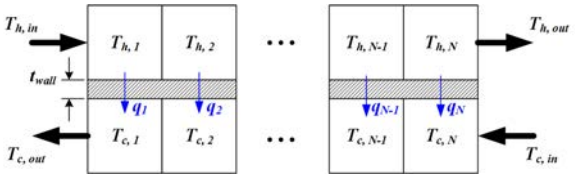

Figure 3: Heat Exchanger Model

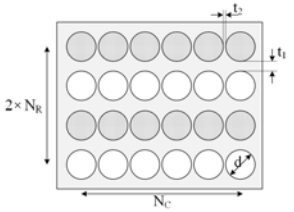

Figure 4: Modelling approximation for Printed Circuit Heat Exchanger

To address this, the heat exchangers are modelled using the approach and software developed by Jahn (2017a,b). Similar to the effective heat transfer approach the heat exchanger is split into multiple axial slices, as shown in Fig. 3, so that quasi constant thermo physical properties can be assumed. Heat transfer in the cross channel direction is then calculated by solving the following set of simultaneous equations

$$q = A_h\, h_h\big(T_h - T_{h,wall}\big), \qquad (9)$$

$$q = A_w\, \frac{k}{t_{wall}}\big(T_{h,wall} - T_{c,wall}\big), \qquad (10)$$

$$q = A_c\, h_c\big(T_{c,wall} - T_c\big), \qquad (11)$$

where h_h and h_c are the local heat transfer coefficients for the h and c channel respectively and A_h, A_w, and A_c are the corresponding heat transfer areas. The model also considers thermal conduction in the axial direction both in the fluid and the wall. Using appropriate parameters for geometry and empirical Nusselt number correlation to obtain heat transfer coefficients this approach can accurately capture the performance of heat exchangers across changing operating conditions.

For the current study the recuperator is taken to be a printed circuit heat exchanger (PCHEX). These have proven to operate well at the higher temperatures and pressures of sCO2 systems as tested by CSIRO (private communications). For modelling their geometry is approximated as shown in Fig. 4, and the heat transfer correlation for sCO_2 by Lia and Zhao (2002) is used. Work by Bone (private communications) shows that this approach accurately captures performance of a sCO_2 PCHEX performance with temperature errors of less than *1K* across multiple operating conditions.

To allow a more direct comparison of the cycles, the current study assumes that the heat source and heat sink heat exchangers are sufficiently large so that constant working fluid outlet temperature can be attained by controlling the heat source or heat sink mass flow rates

Solution Process

The operation of cycles at steady state operating points is evaluated using the SCARR, Jahn (2017c) and Jahn and Keep (2017), which uses non-linear optimisation to solve equations of the form:

$$\min_{x \in R} (\boldsymbol{A}\, x + Y)^2, \quad \text{where} \quad Y = \boldsymbol{F}(\mathrm{x}) \qquad (12$$

where x defines the state points in the cycle (pressure, temperature, mass flow rate), $\boldsymbol{F}$ defines the non-linear functions capturing the component behaviour, and $\boldsymbol{A}$ is a matrix defining additional constraints to ensure a unique solution exists. For the cycles in this paper an additional constraint is that the compressor inlet pressure is fixed to *9MPa*. In practice this would be achieved by employing an appropriate inventory control system. In addition, for the recompression cycle the exit pressures of the two fluid streams joining at the merge are constrained to the same value.

The results from this optimisation process is a set of cycle operating conditions (pressures, temperature, flow rates) that match at the interfaces between all the cycle components. Using the current components models the effects of changing external conditions (e.g. shaft speed) are captured by changing the working line of the compressor or turbine, which is then automatically matched to the rest of the system. Currently the detrimental effect of supporting systems (sealing, cooling systems) is not considered.

RESULTS AND DISCUSSION

To illustrate the operation of SSCAR and to build an understanding of the part-load operation of sCO_2 power systems, this work first considers a recuperated Brayton cycle, before investigating the more complex recompression Brayton cycle.

Recuperated Brayton Cycle

The configuration of a recuperated Brayton cycle is shown in Fig. 5 and the operating conditions at the design point are summarised in Tab. 1. The recuperator is modelled as a PCHEX with a matrix of *100×400*, *1.6mm* diameter channels in parallel and a length of *1.6m*. The compressor model is scaled based on the data from Wright et al (2010) and the turbine on the Ricardo A70 (Hiett and Jonston 1962).

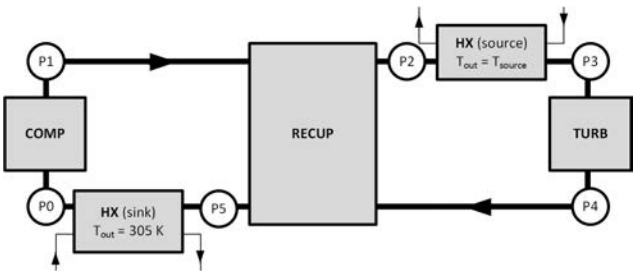

Figure 5: Recuperated closed loop Brayton cycle.

Table 1: Nominal design point for recuperated sCO_2 Brayton cycle (configuration R0)

Parameter	Value	Parameter	Value
T_{So} [K]	883	T_{Si} [K]	305
P Compressor Inlet [MPa]	8.5	Pressure Ratio	2.35
η_C	62%	η_T	80%
N_C	1.0	N_T (fixed)	1.0
m_{Cycle} [kg/s]	10.22		

To illustrate the effect of varying external conditions on cycle performance, the following five cases are investigated: (A) Nominal; (B1/B2) source temperature reduced by *100* and *200K*; and (C1/C2) compressor speed reduced to *0.925* and *0.85*. For all cases the turbine speed is kept constant, corresponding to operation with a synchronous generator. The temperature entropy diagram of the resulting cycle is shown in Fig. 6 and the corresponding recuperator temperature profile is shown in Fig. 7.

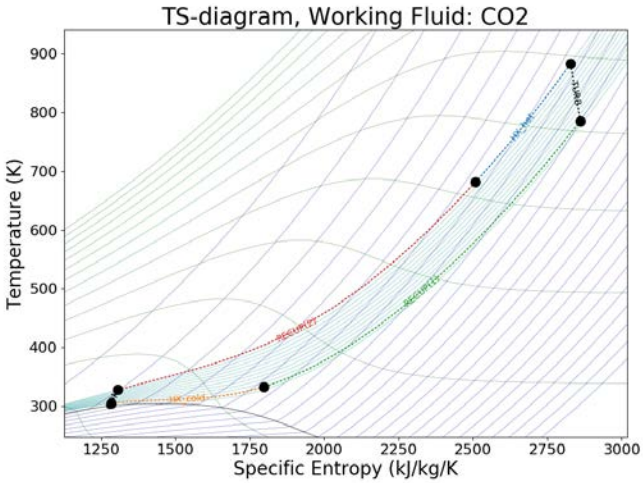

Figure 6: Temperature - entropy diagram for recuperated Brayton cycle (Case R0.A)

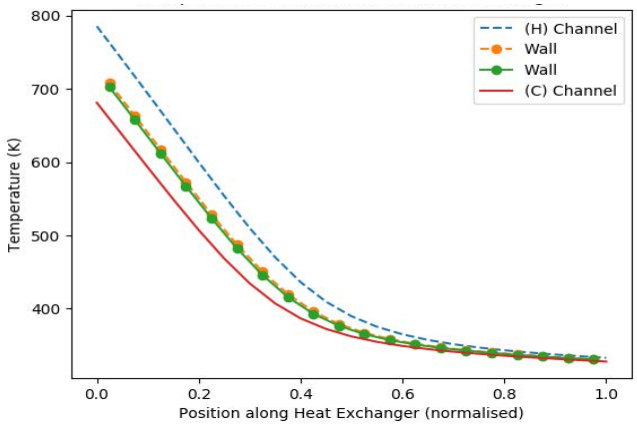

Figure 7: Recuperator temperature profile

Considering these, the importance of efficient recuperation to ensure efficient cycle operation is highlighted. In the proposed cycle the energy exchanged in the recuperator is *5612kW*, compared to a heat addition of only *2547kW*. Likewise Fig. 7 highlights the pinch-point created by the non-linear properties of sCO_2, which result in a temperature difference of almost *100K*, which potentially could be recuperated.

At the design point the recuperated Brayton cycle has a thermal conversion efficiency W_{net}/Q_{in} of 35%, which is 0.53 of the Carnot efficiency. A *+/-10* percentage point change in compressor and turbine efficiency would change this by *+/-2.2* and *+/-4.4* percentage points respectively, as outline by Brun et al. (2017). The comparatively smaller effect of the compressor is to some extend due to the change in compressor exit temperature. A low efficiency compressor (higher exit temp) moves the recuperator pinch point to the left (see Fig. 7) and allow the temperature difference at the recuperator exit to be reduced.

The changes in cycle performance for off-design operation are summarised in Tab. 2 and the corresponding compressor maps and turbine showing the shift in operating points are shown in Fig. 8.

Table 2: Recuperated Brayton cycle, performance parameters as a function of operating conditions

Parameter	R0.A	R0.B1 (T_{Tin}= 783 K)	R0.B2 (T_{Tin}= 683 K)	R0.C1 (N_C= 0.925)	R0.C2 (N_C= 0.85)
$\dot{m}_{cycle}$ [kg/s]	10.22	10.47	11.07	8.68	6.89
P_T [MPa]	20.0	19.94	19.86	18.21	16.32
Q [kW]	2547.1	2432.3	2285.4	2013.2	1438.3
W_C [kW]	237.1	241.7	245.5	173.7	118.3
W_T [kW]	1127.7	997.1	833.8	855.4	570.6
W_{net} [kW]	890.6	755.4	588.3	681.7	452.3
η_{Cycle} [%]	35.0	31.1	25.7	33.9	31.4

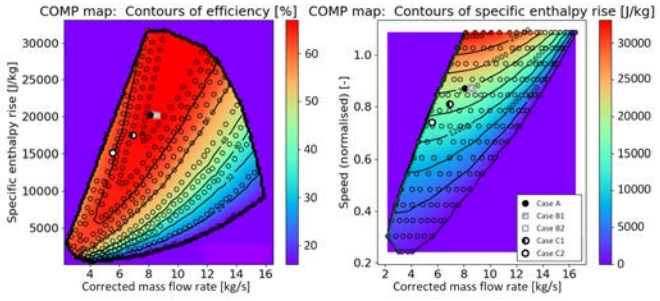

(a)

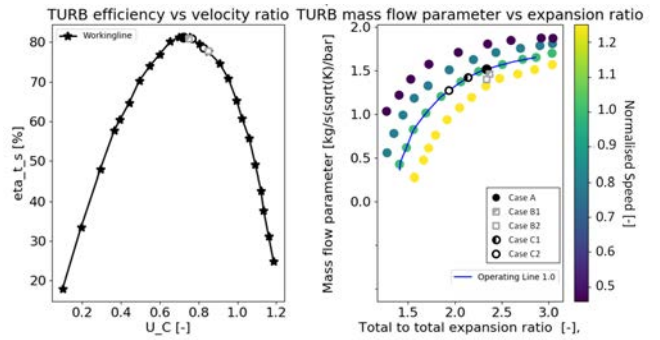

(b)

Figure 8: Maps showing the operating points of the compressor (a) and turbine (b) for the recuperated Brayton Cycle (configuration R0)

Considering the reduction of turbine inlet temperature, a small increase in turbine mass flow rate is observed. However, this increase is outweighed by the reduction in temperature, resulting in a reduction in mass flow parameter and pressure ratio. This is matched by the compressor, which experiences a slight reduction in enthalpy (pressure) rise. Overall these effects are small as shown in Fig. 8. Nevertheless, the impact of the temperature reductions is significant, leading to *4* and *9* percentage point efficiency reductions in cycle efficiency for *100* and *200K* reductions in turbine inlet temperature respectively.

When the compressor speed is reduced, a significant drop in cycle mass flow rate is observed, as shown in Tab. 2. At reduced mass flow rate operation, the compressor operating points shifts towards the surge line, resulting in reduced compressor efficiencies and enthalpy (pressure) rise. The resulting reduction in turbine inlet pressure causes moves the turbine operating point to a lower mass flow

parameter and pressure ratio. However, as spouting velocity is only a weak function of inlet pressure (see Eqn. (6)), the effect on turbine efficiency is minimal as shown in Fig 8(b). Consequently, cycle efficiency remains a *33.9%* and *31.4%* for the respective cases, while at the same time cycle output is reduced to *77* and *51%* of nominal. This highlights the ability of the sCO_2 Brayton cycle to operate at part-load without experiencing significant drop offs in efficiency. For the current cycle configuration is limited to *85%* compressor speed, before the compressor runs into surge. However this operating range could be extended either by shifting the nominal compressor operating point or by the introduction of compressor inlet guide vanes to extend the operating map.

Recompression Brayton Cycle

Currently one of the most promising sCO_2 cycle configurations is the recompression cycle, shown in Fig. 9. Cycle studies by Turchi at al. (2013) showed that this cycle configuration can attain thermodynamic efficiencies in excess of *50%*. While more efficient cycle configurations are feasible (e.g. through introduction of reheat or intercooling), the trend is that the thermodynamic gains are generally outweighed by the added complexity, especially when considering small cycles (*<25MW*). The recompression cycle is realised through the introduction of a re-compressor (RC), and an additional recuperator. This configuration allows the mass flow rate in the cold channel of the low temperature recuperator to be reduced, thereby mitigating the effect of the pinch point that limits recuperation in the Brayton cycle discussed previously.

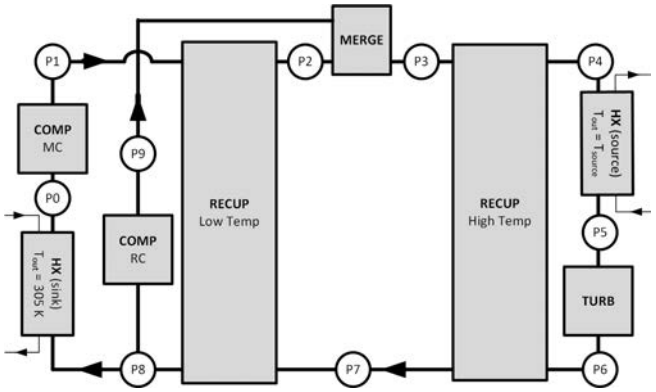

Figure 9: Schematic for closed loop recompression cycle

On-design (Nominal) Performance

To investigate the on and off-design performance of the recompression cycle, two configurations are considered. Configuration R1 uses the turbomachinery efficiencies proposed by Turchi et al. (2013), which are based on works from Dostal (2004). Configuration R2 uses reduced efficiencies, based on the data presented by Brun et al (2017), Clemetoni et al (2015), McDowell et al (2015), US Department of Energy (2015), Wilkes et al (2016) and Wright et al (2010), which are likely to be achieved in first sCO_2 demonstrations. For both recompression cycle configurations the turbine inlet temperature has been set to 610^0C and the nominal output power to *25MW*, which is deemed to be near the limit for radial turbomachinery. In both cases identical printed circuit heat exchangers are used with a matrix of *100×600*, *1.6mm* diameter channels. The length of both recuperators is *7m*. The performance maps of the compressors and turbine are again based on the maps from Wrigth et al (2010) and Hiett and Johnston (1963), but scaled both with respect operating conditions and efficiency. The remaining parameters defining the cycle and nominal operating point are summarised in Tab. 3.

Table 3: Recompression Brayton cycle. Operating conditions and performance at design point.

Configuration	R1	R2
$\dot{m}_T$ [kg/s]	263.1	262.8
T_{Tin} [K]	883	883
T_{Si} [K]	307	307
P_{Tin} [MPa]	19.97	19.95
P_{Cin} [MPa]	9.0	9.0
Split $(\dot{m}_{MC}/\dot{m}_T)$	0.70	0.70
N_{MC} [-]	1.0	1.0
N_{RC} [-]	1.0	1.0
N_T (fixed) [-]	1.0	1.0
η_{MC} [%]	89 %	83%
η_{RC} [%]	89 %	80%
η_T [%]	93 %	85%
η_{Cycle} [%]	47.2	42.8%

The two cycles are nominally the same, however the reduction in turbomachinery efficiencies results in a *4.4* percentage point cycle efficiency penalty. Discrepancies in cycle efficiency between R1A and the data presented by Turchi (2013) arise from the different modelling approach and sizing of the heat exchangers and their respective pressure drops.

The pressure and temperature conditions for case R1A are overlaid on a temperature entropy diagram in Fig. 10. This highlights the respective operating conditions of the two compressors. At these conditions the energy exchanged in the low and high temperature recuperators is *24.1* and *120.8MW* respectively. The cycle also experiences a mismatch in fluid temperature at the merge between the fluid exiting the re-compressor and the low temperature recuperator of *15K*. The result of the mixing process is that the fluid entering the high temperature recuperator is slightly hotter. Further optimisation of the respective recuperator sizes is desirable to establish the ideal temperature difference at the merge, as the mixing process can augments the operation of the high temperature recuperator.

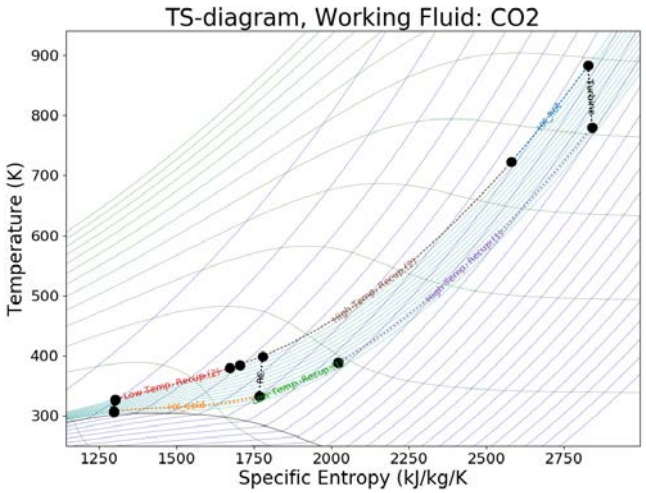

Figure 10: Temperature - entropy diagram for Recompression cycle (Case R1.A)

Off-design Performance

When considering the off-design operation of the recompression cycle the merge is a key feature, as it matches the outlet pressure of the two compressors. As the main compressor and re-compressor have different performance maps this results in a shift of the mass flow rate split ($\dot{m}_{MC}/\dot{m}_T$) with changes in cycle operation. Effectively without an additional variable to control the performance of on or both compressor (e.g. independent speed control or variable inlet vanes) the mass flow split varies.

Table 4: Recompression cycle configuration R1, performance parameters

Parameter	R1.A	R1.B (T_{Tin} = 700 K)	R1.C1 (N_C = 0.925)	R1.C2 (N_C = 0.85)
$\dot{m}_T$ [kg/s]	263.1	274.8	230.1	197.8
$P_{T\,in}$ [MPa]	19.97	19.73	18.32	16.90
$\dot{m}_{MC}/\dot{m}_T$	0.70	0.70	0.67	0.66
ΔT_{Merge} [K]	15.0	23.9	13.2	11.4
Q (in) [MW]	52.2	45.9	41.5	32.7
W_{MC} [MW]	3.13	3.18	2.26	1.61
η_{MC} [%]	89.0	89.0	87.9	86.4
W_{RC} [MW]	3.05	3.17	2.53	1.94
η_{RC} [%]	89.0	89.0	89.0	87.7
W_T [MW]	30.8	23.8	24.2	18.5
η_T [%]	92.2	89.8	92.2	91.2
W_{net} [MW]	24.7	17.4	19.4	15.9
η_{Cycle} [%]	47.2	38.0	46.8	45.9

To provide the insight towards the operation of the recompression cycle at off-design conditions, conditions are simulated corresponding to a reduction in turbine inlet temperature to *700K* (case R1.B/R2.B) and reductions in rotational speed of both compressors to *0.925* and *0.85* (cases R1.C1/R2.C1 and R1.C2/R2.C2). The resulting key cycle performance parameters are listed in Tab. 4 and 5.

Table 5: Recompression cycle configuration R2, performance parameters

Parameter	R2.A	R2.B (T_{Tin} = 700 K)	R2.C1 (N_C = 0.925)	R2.C2 (N_C = 0.85)
$\dot{m}_T$ [kg/s]	262.8	274.6	229.7	189.2
P_{Tin} [MPa]	19.95	19.73	18.30	16.54
$\dot{m}_{MC}/\dot{m}_T$	0.70	0.70	0.67	0.62
ΔT_{Merge} [K]	18.9	24.6	11.8	3.22
Q_{in} [MW]	48.3	42.8	38.4	27.6
W_{MC} [MW]	3.3	3.4	2.4	1.6
η_{MC} [%]	83	83.0	82.0	76.9
W_{RC} [MW]	3.5	3.6	2.8	2.2
η_{RC} [%]	80	80.0	79.9	78.8
W_T [MW]	27.5	21.2	21.5	15.2
η_T [%]	82.26	80.2	82.3	80.9
W_{net} [MW]	20.7	14.2	16.3	11.4
η_{Cycle} [%]	42.8	33.2	42.4	41.4

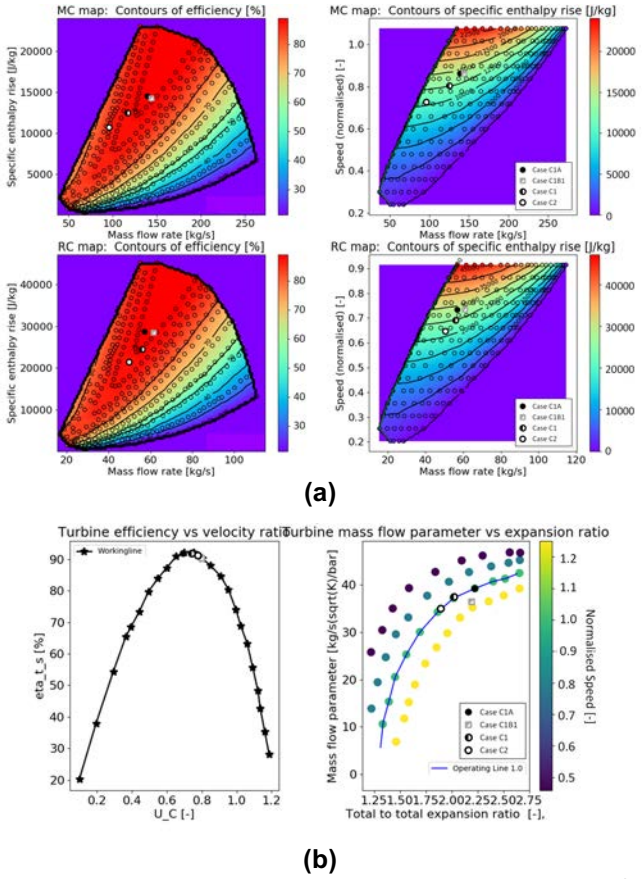

Figure 11: Maps showing the operating points of the compressor (a) and turbine (b) for the recompression Brayton Cycle (configuration R1)

Comparing these data, it is evident that the observed trends for both cycle configurations are nearly identical, albeit the cycle with the lower efficiency components shows a reduction in output power from *24.7* to *20.7MW*. The reduction in efficiency is less significant as the reduced efficiency components allow increased recuperation, which

manifests in a reduction of input power, Q_{in}, from *52.24* to *48.3MW*. The results are cycles with thermodynamic conversion efficiencies of *47.2* and *42.8 %* respectively.

The effect of reducing turbine inlet temperature to *700K* is near identical in both cases. Similar to the recuperated cycle, mass flow rate increases slightly. As conditions at the compression end of the cycle remain almost the same, only a minor shift exists for the compressor operating point is observed, as shown in Fig. 11(a). For the turbine, the reduction in inlet temperature causes a shift to a lower equivalent speed. The corresponding change in velocity ratio causes an approximately *2.3* percentage point reduction in turbine efficiency. However, as turbine work output, W_T, decreases rapidly with inlet temperature, a significant reduction in net work output is observed. The effect of reducing turbine inlet temperature is that cycle efficiency drops by *9.2* and *9.6* percentage points for configurations R1 and R2 respectively.

The impact of reducing the rotational speed of both compressors is much more favourable for cycle efficiency. Similar trends are observed for both cycle configurations. The reduction in compressor speed causes a reduction in cycle mass flow rate and pressure ratio. The effect of this on turbine efficiency is minimal, as the spouting velocity is only weakly affected by the inlet pressure as shown in Fig. 11(b). Different effects are observed for the two compressors. In both cases operating points shift towards the surge line as shown in Fig. 11(a). This is caused by a shift in split ratio $\dot{m}_{MC}/\dot{m}_T$, which sees an increased portion of the mass flow passing through the re-compressor. In relative terms the re-compressor mass flow increases from *30%* to *34%* and *38%* for cycle configurations R1 and R2 respectively. The consequence of this is that the main compressor moves away from the optimum efficiency operating point more rapidly. Consequently, the main compressor efficiency drops by approximately *3-6* percentage points, whereas the re-compressor efficiency only drops by approximately *1.2-1.3* percentage points. However, the net effect on overall cycle efficiency is small. This is the case as power input to compressor and power output from the turbine decreases proportionally. The reductions in cycle efficiency for *0.925* and *0.85* compressor speeds are *0.4* and approximately *1.2* percentage points for the respective cycle configurations. At the same time output power is reduced to *78* and *65%* for the high efficiency component configuration R1 and to *78* and *55%* for the lower efficiency component configuration R2. This highlights that the sCO_2 recompression cycle is even better at part-load operation than the recuperated Brayton cycle presented earlier in this paper.

Currently the maximum turn-down is limited by the main compressor operating point approaching the surge line. This can be avoided through the introduction of variable compressor geometries or through independent speed control of the main and re-compressor, which allows control of the mass flow rate split between the two compressors.

The analysis of the recompression cycle, both with near optimal component efficiencies and reduced component efficiencies that are more typical for small cycles has shown that the cycle experiences a rapid decline in thermodynamic efficiency when the energy supply and thus the turbine inlet temperature is reduced. In contrast compressor speed is an efficient approach to modulate output power. Using the compressor speed alone, without any additional changes to the system allows the net power output of the cycle to be halved. At the same time thermal conversion efficiency reduces by less than *2* percentage points. This trend arises due to the high levels of recuperation employed, which ensures that thermal energy is recovered. This highlights the suitability of the sCO_2 recompression cycle for applications that substantially operate away from the nominal design point. As such the simple recuperated Brayton cycle and even more so the recompression Brayton cycle are highly suitable for island grid or fringe of grid applications, or applications in networks with a high penetration of PV and wind. In such settings the sCO_2 cycles can perform a load following role across a wide range of output power, while minimising usage of the energy resource. This can be especially advantageous in applications using thermal storage as the hear source (e.g. concentrated solar thermal) as it allows the storage size to be kept small.

The results presented herein are based on scaled experimental data from similar radial compressors and turbines. However, as the underlying effects that cause losses are invariant the general shape of performance maps will remain. Thus trends presented herein will continue to apply.

Future work, once the confidence of numerical simulations of sCO_2 devices has been established will seek to replace these empirical maps, which appropriate numerical ones.

CONCLUSIONS

Numerical models for an *890kW* recuperated sCO_2 Brayton cycle and two variants of a *25MW* recompression sCO_2 Brayton cycle have been presented. These cycle models use scaled experimentally determined performance maps to capture the operation of the centrifugal compressors and radial inflow turbines. The heat exchangers are modelled using physics based approximations using appropriate Nusselt number correlations. Using this performance map based approach allows model boundary conditions to be perturbed and the corresponding changes in cycle operation to be investigated.

Numerical experiments have revealed that changing compressor speed is an effective way to modulate the cycle output power. For the various cycles reducing the compressor speed to *85%* of nominal results in a power reduction to approximately *55%* of nomincal. However, at the same time the cycle efficiency only reduces by 1.4 and 3.5 percentage points for the recompression and recuperated sCO_2 cycles respectively. This highlights the ability of the sCO_2 cycle to operate across a wide range of output power while maintaining a high output efficiency. In contrast reducing the source or turbine inlet temperature leads to significant reductions in cycle efficiency (approximately *9* percentage points for a *180K* reduction) and is not suitable for output power modulation.

This confirms the desirable requirement to operate sCO_2 cycles from a near constant temperature heat source. It also highlights the ability of the cycle to be used for applications that require substantial operation at reduced output power. Here the cycle excels as it can operate across a wide power range with only minimal changes in efficiency.

NOMENCLATURE

A – area [m^2]
h – heat transfer coefficient [$W\ m^{-2}\ K^{-1}$]
k – thermal conductivity [$W\ m^{-1}\ K^{-1}$
m – mass flow rate [kg/s]
N – Rotational speed (normalised) [-]
P – Pressure [MPa]
Q – heat flux [kW/MW]
T – temperature [K]
W – work [kW/MW]
η – efficiency [%]

Subscripts
C – Compressor
c – heat exchanger cold channel
h – heat exchanger hot channel
MC – Main compressor
RC – Re-compressor
Si – Heat sink
So – Heat source
T – Turbine
w – wall

ACKNOWLEDGMENTS

This research was supported by the Australian Solar Thermal Research Institute (ASTRI), a project supported by the Australian Government.

REFERENCES

[1] Aghaeimeybodi M., Beath A. (2016). Impact of cost uncertainties and solar data variations on the economics of central receiver solar power plants: An Australian case study. Renewable Energy, 93, 510-524.
[2] Angelino G. (1968). Carbon Dioxide Condensation Cycles for Power Production. Journal of Engineering for Power 90 (3) 287-295.
[3] ASTRI (2012). Australian Solar Thermal Research Initiative. www.astri.org.au
[4] Bell I.H., Wronski J., Quoilin S., Lemort V. (2014). Pure and pseudo-pure thermophysical property evaluation and the open-source thermophysical property library coolprop. Industrial & engineering chemistry research, 53(6):2498
[5] Balje O.E. (1962). A study on Design Criteria and Matching of Turbomachines: Part A – Similarity Relations and Design Criteria of Turbines, Journal of Engineering for Power, Jan 1962, 83-102
[6] Brun K., Friedman P., Dennis R. (2017). Fundamentals and Application of Supercritical Carbon Dioxide (sCO_2) Based Power Systems. Woodhead Publishing, ISBN:978-0-08-100804-1
[7] Clementoni E.M., Cox T.L., King M.A. (2015). Off-nominal component performance in a supercritical carbon dioxide Brayton cycle. In: Proc. ASME Turbo Expo GT2015-42501, Montreal, Canada.
[8] Denholm P., Hand M. (2011). Grid flexibility and storage required to achieve very high penetration of variable renewable electricity. Energy Policy 39 (2011) 1817–1830
[9] Dostal V. (2004). A Supercritical Carbon Dioxide Cycle for Next Generation Nuclear Reactors, PhD thesis, Massachusetts Institute of Technology
[10] Duniam A., Veeraragavan A. (2017). Off-design performance modeling of the supercritical carbon dioxide recompression Brayton cycle for CSP. In: Solar Paces 2017.
[11] Glassman A.J. (1972). Turbine design and application. NASA Special Publication , NASA SP-290.
[12] Held T.J. (2014). Initial test results of a MegaWatt-class supercritical CO_2 heat engine. In: 4th International sCO_2 Power Cycle Symposium, Pittsburgh, PA.
[13] Hiett G.F., Johnston I.H. (1963). Paper 7: Experiments concerning the aerodynamic performance of inward flow radial turbines. In Proceedings of the Institution of Mechanical Engineers, Conference Proceedings, volume 178, pages 28
[14] Jahn I.H.J. (2017a). Code for the design and evaluation of heat exchangers for complex fluids, School of Mechanical and Mining Engineering, Technical Report, The University of Queensland
[15] Jahn I.H.J. (2017b). Code for the design and evaluation of heat exchangers for complex fluids, Journal for Open Research Software (in press)
[16] Jahn I.H.J. (2017c). SSCAR – Steady State Cycle AnalyseR, School of Mechanical and Mining Engineering, Technical Report, The University of Queensland
[17] Jahn I.H.J., Keep J.A. (2017). Steady State Cycle Ananlyser. Journal for Advances in Engineering Software (in press)
[18] Liao S.M., Zhao T.S. (2002), An experimental investigation of convection heat transfer to supercritical carbon dioxide in miniature tubes, International Journal of Heat and Mass Transfer, 45,
[19] Luu M.T., Milani D., McNaughton R., Abbas A. (2017). Analysis for flexible operation of supercritical CO_2 Brayton cycle integrated with solar thermal systems. Energy 124 (2017) 752e771
[20] McDowell M., Eastland A., Huang, M. Swingler C. (2015). Advanced Turbomachinery for sCO_2 Power Cycles. In: NETL: University Turbine System Research Workshop, Atlanta, GA
[21] Moore J., Brun K., Evans N., Kalra C. (2015). Development of a 1 MWe supercritical CO_2 test loop. In: Proc. ASME Turbo Expo GT2015-43771, Montreal, Canada.
[22] NPSS (2017). Numerical Propulsion System Simulation, South West Research Institute,

http://www.swri.org/consortia/numerical-propulsion-system-simulation-npss
[23] Sauret.
[24] Turchi C.S., Ma Z., Neises T.W., Wagner M.J. (2013), Thermodynamic Study of Advanced Supercritical Carbon Dioxide Power Cycles for Concentrating Solar Power Systems, Journal of Solar Energy Engineering, NOVEMBER 2013, Vol. 135, DOI: 10.1115/1.4024030
[25] United Nations (2015). Framework Convention on Climate Change. Adoption of the Paris Agreement. Technical Report, Paris.
[26] U.S. Department of Energy, (2015). Recuperator Technology Development and Assessment for Supercritical Carbon Dioxide (sCO_2) Based Power Cycles. NETL Funding Opportunities Announcement DE-FOA-0001239, Washington, DC.
[27] Whitfield A., Baines N.C. (1990). Design of radial turbomachines. Longman Scientific & Technical, ISBN: 978-0582495012
[28] Wilkes J., Allison T., Schmitt J., Bennett J., Wygant K., Pelton R., Bosen W. (2016). Application of an integrally geared compander to an sCO_2 recompression Brayton cycle. In: The 5th International Symposium – Supercritical CO_2 Power cycles, San Antonio, TX.
[29] Wright S.A., Radel R.S, Vernon M.E., Rochau G.E., Pickard P.S. (2010). Operation and Analysis of a Supercritical CO_2 Brayton Cycle, SANDIA report, SAND2010-0171